The Thermodynamic Limit of Indoor Photovoltaics Based on Energetically-Disordered Molecular Semiconductors

Kay, Austin M.; Fitzsimons, Maura E.; Burwell, Gregory; Meredith, Paul; Armin, Ardalan; Sandberg, Oskar J.

The Thermodynamic Limit of Indoor Photovoltaics Based on Energetically-Disordered Molecular Semiconductors

Austin M. Kay, Maura E. Fitzsimons, Gregory Burwell, Paul Meredith, Ardalan Armin,* and Oskar J. Sandberg*

Due to their tailorable optical properties, organic semiconductors show considerable promise for use in indoor photovoltaics (IPVs), which present a sustainable route for powering ubiquitous "Internet-of-Things" devices in the coming decades. However, owing to their excitonic and energetically disordered nature, organic semiconductors generally display considerable sub-gap absorption and relatively large non-radiative losses in solar cells. To optimize organic semiconductor-based photovoltaics, it is therefore vital to understand how energetic disorder and non-radiative recombination limit the performance of these devices under indoor light sources. In this work, we explore how energetic disorder, sub-optical gap absorption, and non-radiative open-circuit voltage losses detrimentally affect the upper performance limits of organic semiconductor-based IPVs. Based on these considerations, we provide realistic upper estimates for the power conversion efficiency. Energetic disorder, inherently present in molecular semiconductors, is generally found to shift the optimal optical gap from 1.83 to ≈1.9 eV for devices operating under light emitting diode spectra. Finally, we also describe a methodology (accompanied by a computational tool with a graphical user interface) for predicting IPV performance under arbitrary illumination conditions. Using this methodology, we estimate the indoor power conversion efficiencies of several photovoltaic materials, including the state-of-the-art systems PM6:Y6 and PM6:BTP-eC9.

1. Introduction

A recent coalescence of several technological trends has led to rapid developments in low-power networked devices, collectively referred to as the "Internet-of-Things" (IoT), which are poised to

revolutionize almost all sectors of the global economy.[1,2] While many of these devices may consume less than a microwatt of power, their aggregate energy consumption and environmental footprint must be carefully considered as they become ubiquitous in our homes and workspaces.[3–7] In this regard, indoor photovoltaics (IPVs) have emerged as a very attractive alternative for powering IoT devices.[8] The development of IPVs is propelled by progress in efficient charge controllers and supercapacitors, extending their viability for powering IoT devices to situations where illumination is not continuous.[9] Additionally, the lower light intensities and milder environments usually present indoors also provide less challenges for developing IPVs with enhanced longevities.[8,10]

From a material optimization perspective, the criteria that IPVs are benchmarked against differ in several ways from those used for conventional photovoltaics. These differences stem from the fact that the emission spectra and irradiances of sources of artificial light, such as light-emitting diodes (LEDs), are quite unlike the standard AM1.5G spectrum of sunlight. In general, the spectral emission peaks of artificial light sources are narrower and centered at higher photon energies than the sunlight spectrum, and their integrated irradiances are usually at least three orders of magnitude lower. Because of these differing spectral characteristics, the optimal semiconductor energy gap needed for IPV applications is generally between 1.7 and 1.9 eV, which is considerably wider than the bandgaps of conventional materials like crystalline silicon (1.1 eV), gallium arsenide (1.42 eV), and cadmium telluride (1.44 eV).[11] For a given spectrum, the optimal gap and power conversion efficiency (PCE) is commonly estimated using the Shockley-Queisser (SQ) model. Under typical indoor conditions, the SQ model predicts PCEs surpassing 50% in single-junction devices with optimal energy gaps – significantly larger than the predicted PCE of 33.7% for AM1.5G sunlight.[12,13] To achieve such theoretically-high PCEs, alternative wide-gap semiconductors are urgently needed for use in indoor applications. Next-generation, molecular semiconductors exhibit several attributes that make them desirable for such applications, including mechanical and form factor flexibility, low embodied energy manufacturing, and the

A. M. Kay, M. E. Fitzsimons, G. Burwell, P. Meredith, A. Armin, O. J. Sandberg
Sustainable Advanced Materials (Sêr-SAM)
Centre for Integrative Semiconductor Materials (CISM)
Department of Physics
Swansea University Bay Campus
Swansea SA1 8EN, UK
E-mail: ardalan.armin@swansea.ac.uk; o.j.sandberg@swansea.ac.uk

fact that they are amenable to solution-based fabrication techniques like spin-coating and roll-to-roll printing.[14,15] Of these, organic semiconductors are of particular technological-relevance for indoor applications because of the vast palette of materials available and the tunability afforded by synthetic organic chemistry.[16–19]

In recent years, the performance of organic photovoltaics (OPVs) based on combinations of polymeric donors and low-offset, non-fullerene (small molecule) acceptors (NFAs) has advanced considerably.[20–25] OPV materials and device architectures, however, are not yet optimized for indoor applications, due in part to the relative infancy of the field and the lack of established measurement standards.[26–28] Furthermore, the maximum, experimentally-determined PCE reported for an IPV device based upon conventional OPV principles is currently around 31%, whereas typical PCEs are on the order of 20% – considerably lower than the thermodynamic limit calculated via the SQ model.[29,30] A thorough investigation of the realistic thermodynamic limits of existing OPVs for indoor applications is therefore required for two reasons. Firstly, such an investigation would provide a roadmap for next-generation IPV development, including which routes for device optimization should be pursued. Secondly, it would provide a benchmark for IPV device characterization – until relevant standards are established, inter-laboratory comparisons are complicated by sources of uncertainty and error.[26] These include variations in the spectra and irradiances used to simulate indoor illuminations – all too common problems encountered in the early days of organic solar cells designed for outdoor power generation, but re-emerging now for IPVs.

To obtain realistic predictions for the maximum PCEs and optimal gaps of IPVs based on organic semiconductors, the associated loss mechanisms of OPV devices must be audited.[9] This includes accounting for the excitonic nature of OPVs, as well as the associated static disorder that correlates with a broadened absorption onset and increased sub-gap absorption.[31–33] In general, absorption well below the optical gap induces radiative losses in the open-circuit voltage. Sub-gap absorption is typically correlated with the so-called Urbach energy (E_U) – a measure of the exponential decay in absorption with decreasing photon energy (E).[34,35] As a result, OPVs with lower energetic disorder and smaller E_U are likely to have reduced open-circuit voltage losses and, consequently, higher PCEs.[22,36–38] In addition to the radiative open-circuit voltage losses induced by sub-gap absorption, further non-radiative open-circuit voltage losses are present in OPVs due to the intrinsic prevalence of non-radiative recombination.[39–41] The electroluminescent external quantum efficiency (EQE_{EL}) is commonly used to estimate these non-radiative open-circuit voltage losses.[42] While numerous processes can contribute to the non-radiative recombination in OPVs, the associated voltage loss has been found to generally correlate with the energy gap.[39,41]

In this work, we step beyond the rudimentary SQ model to make realistic predictions for the PCEs of existing OPVs in indoor settings. We explore the effects of the optical gap and energetic disorder on the optimal PCE. In addition, we investigate the role of non-radiative open-circuit voltage losses, while accounting for the energy gap-dependence of non-radiative recombination using an optimistic-yet-realistic empirical model

guided by literature OPV data. Following this, we present a methodology and an accompanying computational tool (with an accessible graphical user interface) for recontextualizing a given photovoltaic system's existing measurements under one-Sun conditions to predict how it might perform under arbitrary illumination conditions. Utilizing this methodology, which employs measurements of a device's photovoltaic external quantum efficiency spectrum and its open-circuit voltage under AM1.5G conditions, we predict the indoor performance of dozens of emerging OPV systems. Finally, we demonstrate that the "fruit fly" systems PM6:Y6 and PM6:BTP-eC9 are likely limited to PCEs below 20% in indoor settings.

2. Results and Discussion

2.1. Photovoltaic Figures-of-Merit

The spectral fingerprints of sources of artificial light generally differ from source to source, displaying variations in intensity and separation of emission peaks. In **Figure 1**a, the spectral photon flux densities (Φ_{source}) of typical indoor light sources, including the 'warm white' 2700 K LED and 'cool white' 4000 K LED, are illustrated alongside the International Commission on Illumination's (CIE's) standard illuminant LED-B4. Therein, the integrated power density of each source, $P_{source} = \int_0^\infty E\Phi_{source}(E)dE$, is scaled to a total illuminance of 500 lux (see Section S1 of the Supporting Information). The corresponding scaled AM1.5G spectrum has been included for comparison. In this work, we primarily consider the CIE LED-B4 standard as the indoor light source since as LEDs are becoming more commonplace in most indoor settings. However, it should be noted that the obtained findings are largely independent of the used LED source; similar results are found for the 2700 K LED and 4000 K LED spectra (see Supporting Information). Additional discussions for other standard indoor light sources, including the CIE FL-2, CIE FL-7, and CIE FL-11 spectra, are also available in the Supporting Information.[43,44]

Under illumination, a photovoltaic device will generate power at efficiency[11]

$$PCE = \frac{FF\,J_{sc}\,V_{oc}}{P_{source}} \tag{1}$$

Here, V_{oc} is the open-circuit voltage, J_{sc} is the short-circuit current density, and FF is the fill factor. In general, the open-circuit voltage and the short-circuit current density relate to the device's photovoltaic external quantum efficiency $EQE_{PV}(E)$ (the ratio of the number of collected charge carriers to the number of incident photons at a given photon energy E) via[11]

$$V_{oc} = \frac{kT}{q}\ln\left[1 + \frac{J_{sc}}{J_0(V_{oc})}\right] \tag{2}$$

$$J_{sc} = q\int_0^\infty EQE_{PV}(E)\,\Phi_{source}(E)dE \tag{3}$$

Wherein k denotes the Boltzmann constant, q the elementary charge, and T the temperature. The quantity J_0, on the other hand,
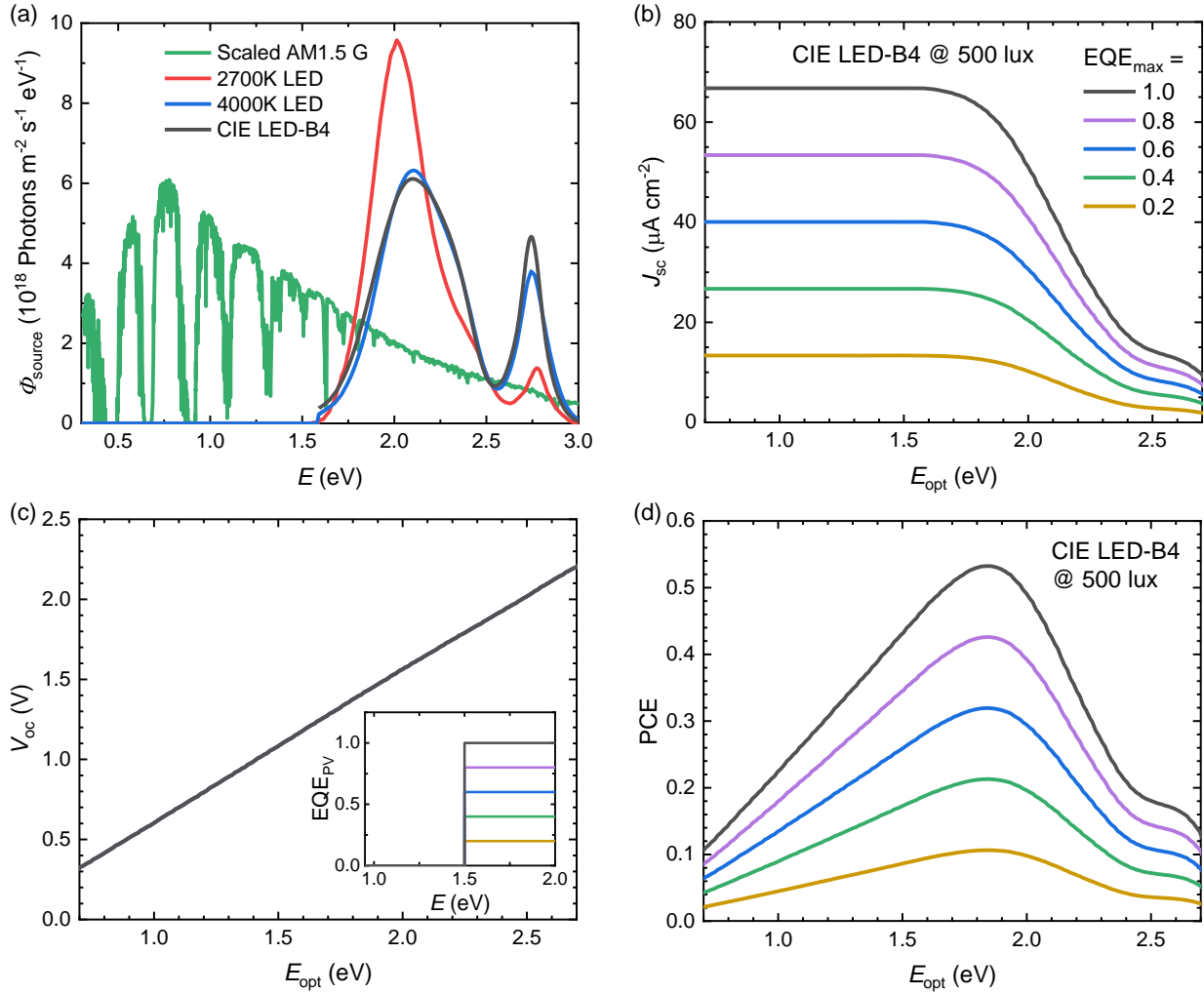
Figure 1. a) The scaled AM1.5G spectrum for sunlight (green), the 2700 K LED spectrum (red), the 4000 K LED spectrum (blue), and the CIE LED-B4 spectrum (black), all plotted against the photon energy at an illuminance of 500 lux. In b–d), the short-circuit current density, the open-circuit voltage, and the power conversion efficiency in the radiative limit under the LED-B4 spectrum at 500 lux, are plotted against the optical gap for varied EQE_{max}, assuming the step-function model for EQE_{PV} given by Equation (7). The effect of increasing EQE_{max} is illustrated for an optical gap $E_{opt} = 1.5$ eV in the inset graph in (c).

is the dark saturation current density. It is calculated using $J_0(V) = J_0^{rad}(V)/EQE_{EL}$, where the radiative dark saturation current density (J_0^{rad}) is defined by[42]

$$J_0^{rad}(V) = q \int_0^\infty EQE_{PV}(E) \, \Phi_{bb}(E) w(E,V) \mathrm{d}E \qquad (4)$$

where $\Phi_{bb}(E) = \frac{2\pi E^2}{h^3 c^2} \exp\left(-\frac{E}{kT}\right)$ is the spectral photon flux density of the ambient black-body radiation at thermal equilibrium (h is the Planck constant and c is the speed of light). Here, $w(E,V)$ is a degeneracy factor accounting for state-filling effects;[36] in the thermodynamic limit, $w(E,V)$ can be approximated as (see Section S3 of the Supporting Information)

$$w(E,V) = \frac{1}{\left[1 + \exp\left(\frac{qV-E}{2kT}\right)\right]^2} \qquad (5)$$

For above-gap states ($E \gg qV$) the non-degenerate limit, $w(E,V) = 1$, typically applies and J_0^{rad} is independent of the voltage. For the general case, however, J_0^{rad} depends on the voltage and an iterative approach must be used to evaluate Equation (2) (again, see Section S3 of the Supporting Information). Note that the device's EQE_{EL} equals one in the radiative limit, giving $J_0 = J_0^{rad}$ while $V_{oc} = V_{oc}^{rad}$ (V_{oc}^{rad} is the corresponding radiative V_{oc}). Photovoltaic devices are generally far from the radiative limit; non-radiative recombination increases J_0 which, in turn, reduces the open-circuit voltage as $V_{oc} = V_{oc}^{rad} - \Delta V_{oc}^{nr}$, where ΔV_{oc}^{nr} is the associated non-radiative open-circuit voltage loss given by $\Delta V_{oc}^{nr} = -\frac{kT}{q}\ln(EQE_{EL})$ for $V_{oc} \gg kT/q$.[42]

Finally, we assume that the current density is approximated by $J = -J_{sc} + J_0^{rad}(V)\exp\left(\frac{q\Delta V_{oc}^{nr}}{kT}\right)\left[\exp\left(\frac{qV}{kT}\right) - 1\right]$, where J_{sc} is given by Equation (3) and $J_0^{rad}(V)$ by Equation (4), corresponding to the

case of ideal charge collection. Subsequently, the FF and the PCE are determined numerically using the iterative approach outlined in Section S3 of the Supporting Information. However, we note that for $w = 1$ (and assuming V_{oc} larger than 0.5 V), the fill factor is well-approximated by[45]

$$\text{FF} \approx \frac{\frac{qV_{oc}}{kT} - \ln\left(1 + \frac{qV_{oc}}{kT}\right)}{1 + \frac{qV_{oc}}{kT}} \quad (6)$$

This suggests that, in the case of ideal charge transport, the leading-order behavior of the fill factor is primarily determined by the open-circuit voltage. Consequently, minimizing open-circuit voltage losses is of paramount importance for realizing high-PCE IPVs based on organic semiconductors. We note, however, that in reality the FF is influenced further by several additional factors; most notably the shunt resistance plays a crucial role in limiting the FF under low light indoor conditions.[8]

2.2. Effect of Radiative Open-Circuit Voltage Losses

We now consider the influence of radiative open-circuit voltage losses on the performance of IPVs by first discussing the idealized case of a sharp optical gap and no sub-gap absorption. In this case, EQE$_{PV}$ can be modelled using a step function, where all photons of energy greater than or equal to a threshold optical gap (E_{opt}) generate a collected electron-hole pair at efficiency EQE$_{max}$, whereas photons of energy less than the optical gap do not

$$\text{EQE}_{PV}(E) = \begin{cases} \text{EQE}_{max}, & \text{if } E \geq E_{opt} \\ 0, & \text{otherwise} \end{cases} \quad (7)$$

The photovoltaic external quantum efficiency in the SQ model is defined by this equation in the ideal case that EQE$_{max} = 1$.[13] For an EQE$_{PV}$ spectrum modeled using Equation (7), the short-circuit current density, radiative open-circuit voltage, and resultant PCE under the CIE LED-B4 spectrum at 500 lux are shown for varying EQE$_{max}$ in Figure 1b–d, respectively. As shown, at a particular optical gap, the short-circuit current density is directly proportional to EQE$_{max}$. The open-circuit voltage, however, is independent of EQE$_{max}$ and so the V_{oc} curves are perfectly aligned and equal to the open-circuit voltage predicted by the SQ model (V_{oc}^{SQ}), which can be approximated as[45]

$$qV_{oc}^{SQ} \approx E_{opt} - kT \ln\left[\frac{2\pi q}{h^3 c^2} \frac{E_{opt}^2 kT}{J_{sc}^{SQ}}\right] \quad (8)$$

for $qV_{oc}^{SQ} \ll E_{opt}$, where $J_{sc}^{SQ} = q \int_{E_{opt}}^{\infty} \Phi_{source}(E) dE$. Note that since the FF is determined by the V_{oc} in this case, the PCE, similar to J_{sc}, scales linearly with EQE$_{max}$; while the E_{opt} dependence of the PCE below the optimal gap is entirely determined by the V_{oc}.

From Figure 1d, it is evident that in the SQ model, the maximum PCE under the CIE LED-B4 spectrum at 500 lux is 53%, obtained at an optical gap $E_{opt} = 1.83$ eV, with $V_{oc}^{SQ} = 1.41$ V

and $J_{sc}^{SQ} = 62.1 \, \mu\text{A cm}^{-2}$. However, for current state-of-the-art OPVs, the empirical upper limit of the EQE$_{PV}$ is closer to 0.85. Therefore, to realistically estimate the PCEs of IPVs based on organic semiconductors, an above-gap photovoltaic quantum efficiency of EQE$_{max} = 0.85$ is herein assumed – unless explicitly stated otherwise – as this value describes realistically-high performance. The corresponding maximum PCE for EQE$_{max} = 0.85$ is reduced to 45.3%, which is still obtained at $E_{opt} = 1.83$ eV (for CIE LED-B4 at 500 lux).

Despite being rudimentary, the step-function model given by Equation (7) is a good approximation for EQE$_{PV}$ in semiconductors with well-defined band edges, such as crystalline, inorganic semiconductors. Many photovoltaic materials, however, are not well-described by the highly-idealized step-function model. A more realistic prediction for the PCEs of IPVs based on energetically-disordered materials, including OPVs, must account for the inherent, static energetic disorder associated with the density of states. As increased static energetic disorder broadens the effective band edges and leads to increased sub-gap absorption, it will increase radiative open-circuit voltage losses and reduce the PCE.

Sub-gap absorption in disordered materials is commonly described by a tail that decays exponentially with decreasing photon energy below the gap. This tail may be designated a characteristic energy – the aforementioned Urbach energy (E_U).[35] Consequently, a more realistic model for EQE$_{PV}$ in many photovoltaics is given by

$$\text{EQE}_{PV}(E) = \text{EQE}_{max}\begin{cases} 1, & \text{if } E \geq E_{opt} \\ \exp\left(\frac{E - E_{opt}}{E_U}\right), & \text{otherwise} \end{cases} \quad (9)$$

The Urbach energy correlates with the level of disorder in a system and, as illustrated in **Figure 2**a, it determines the gradient of the exponential decay of the sub-gap tail. A reasonable minimum value for the Urbach energy of OPVs is the thermal energy (kT); throughout the remainder of this work we assume $kT = 25.3$ meV (corresponding to $T = 20\,°\text{C} = 293.15$ K).[31]

The presence of sub-gap Urbach tails gives rise to a decrease in V_{oc}^{rad}, as shown in Figure 2b. In Figure 2c, it is shown that these losses, in turn, reduce the maximum power conversion efficiency from 45% to around 33% (in the $E_U = 50$ meV case), while concurrently blue-shifting the best-performing E_{opt} from 1.83 to 1.91 eV. Material systems with high E_U therefore require larger optical gaps to achieve high performance. We note that the short-circuit current density is found to be largely independent of E_U. The loss in PCE shown in Figure 2c is therefore a result of the radiative open-circuit voltage loss ($\Delta V_{oc,sub-gap}^{rad}$) induced by sub-gap tails. This voltage loss is quantified by the deviation between V_{oc}^{SQ} (determined in the SQ model) and the V_{oc}^{rad} obtained in case of a sub-gap tail, $\Delta V_{oc,sub-gap}^{rad} = V_{oc}^{SQ} - V_{oc}^{rad}$. For the open-circuit voltage curves of Figure 2b, these deviations were determined then plotted in Figure 2d. For $E_U \geq kT$, the optical gap-dependent behavior of these curves can be described by the following analytical approximations (see Supporting Information)
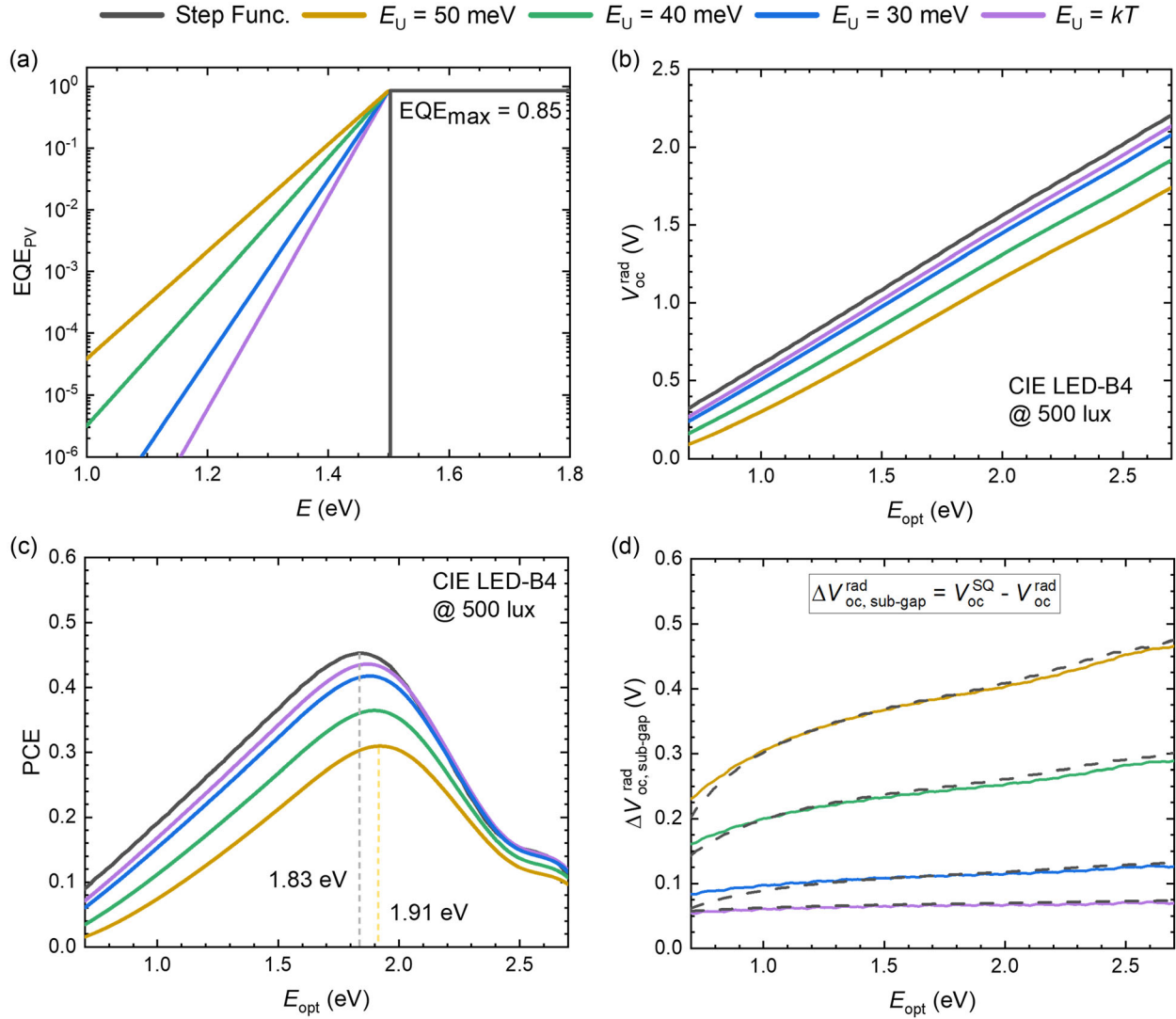
Figure 2. Investigating the effect of sub-gap tails of varying Urbach energy on the open-circuit voltage and the power conversion efficiency. a) Photovoltaic external quantum efficiency spectra centered at an optical gap $E_{opt} = 1.5$ eV, with $EQE_{max} = 0.85$ and E_U varied from 0 (step function) to 50 meV. b) The resultant open-circuit voltages in the radiative limit, plotted as a function of the optical gap. c) The PCE under the CIE LED-B4 spectrum at 500 lux, plotted as a function of the optical gap for a variety of Urbach energies. d) The solid curves indicate the numerically-calculated deviations between the open-circuit voltage in the SQ model and the sub-gap Urbach tail model. The dashed lines indicate the corresponding analytical approximation given by Equation (10).

$$
q\Delta V_{oc,\,sub-gap}^{rad} \approx
\begin{cases}
\left(\frac{E_U}{kT} - 1\right)\left(E_{opt} - qV_{oc}^{SQ}\right) + E_U \ln\left[\frac{\left(\frac{qV_{oc}}{E_{opt}}\right)^2}{1 - \frac{kT}{E_U}}\right], & \text{if } E_U > kT \\[2em]
kT\ln\left[\frac{E_{opt}}{3kT} + 1\right] + kT\ln\left[1 - \left(\frac{qV_{oc}}{E_{opt}}\right)^3\right], & \text{if } E_U = kT
\end{cases}
\tag{10}
$$

Equation (10) describes the behavior of $\Delta V_{oc,\,sub-gap}^{rad}$ for $E_U \geq kT$ at typical optical gaps, as shown by the dashed curves in Figure 2d. We note that, in accordance with Equation (10), for $E_U > kT$ the associated radiative open-circuit voltage displays a $V_{oc}^{rad} \propto \frac{E_U}{kT} V_{oc}^{SQ}$ type dependence. This translates to a radiative ideality factor above unity, consistent with previous reports.[46,47]

In the past, the static energetic disorder in organic semiconductors has also been frequently modelled in terms of a Gaussian distribution of states. Consistent with this, the EQE_{PV} associated with excitonic sub-gap absorption in several low-offset NFA OPV
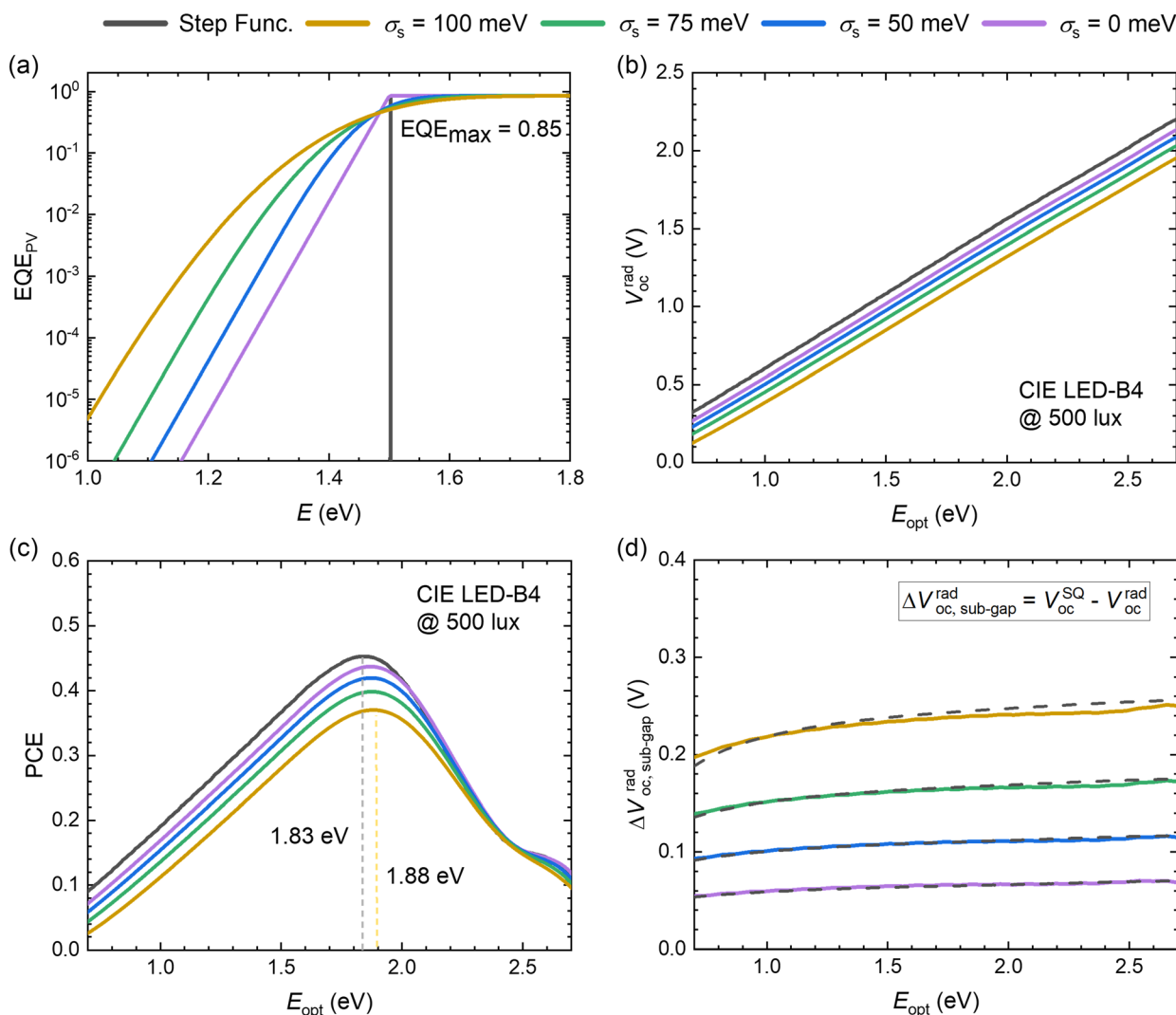
Figure 3. Investigating the effect of energetic disorder on the open-circuit voltage and the power conversion efficiency. a) Photovoltaic external quantum efficiency spectra centered at an optical gap $E_{opt} = 1.5$ eV, with $EQE_{max} = 0.85$ and σ_s varied from 0 to 100 meV, plotted alongside the step function model for EQE_{PV} (in black). b) The resultant open-circuit voltages in the radiative limit, plotted as a function of the optical gap. c) The PCE under the CIE LED-B4 spectrum at 500 lux, plotted as a function of the optical gap for varying σ_s. d) The solid curves indicate the numerically-calculated deviations between the open-circuit voltage in the SQ model and the OPV model, where EQE_{PV} is modelled in the latter using Equation (11). The dashed lines indicate the analytical approximation given by Equation (12).

material systems was recently found to be well-described by[31,33]

$$EQE_{PV}(E) = \frac{EQE_{max}}{2}$$

$$\left\{ \exp\left[\frac{E - E_{opt} + \frac{\sigma_s^2}{2kT}}{kT}\right] \text{erfc}\left[\frac{E - E_{opt} + \frac{\sigma_s^2}{kT}}{\sigma_s\sqrt{2}}\right] + \text{erfc}\left[\frac{E_{opt} - E}{\sigma_s\sqrt{2}}\right] \right\} \quad (11)$$

where E_{opt} is the centre of a Gaussian distribution of exciton states with static disorder parameter σ_s. Here, erfc(x) denotes the complementary error function. The spectral behavior of Equation (11) at different σ_s is illustrated in **Figure 3**a for $EQE_{max} = 0.85$ and an optical gap of 1.5 eV. For energies well below the gap ($E \ll E_{opt}$), Equation (11) reduces to a sub-gap

Urbach tail with $E_U = kT$. Above the gap, on the other hand, a saturation is reached wherein $EQE_{PV}(E) \rightarrow EQE_{max}$. Between these two regimes lies a transition regime with a shape and spectral broadness determined by σ_s.

Figure 3b,c show the V_{oc}^{rad} and PCE as a function of the optical gap, obtained using the EQE_{PV} spectra from Figure 3a. The corresponding radiative open-circuit voltage losses $\Delta V_{oc,sub-gap}^{rad}$, induced by the sub-gap EQE_{PV}, are shown in Figure 3d. As illustrated throughout Figure 3, a higher static energetic disorder gives rise to increased radiative open-circuit voltage loss, thereby reducing the power conversion efficiency from 45% in the step function model to 37% in the $\sigma_s = 100$ meV case. In addition, the best-performing optical gap is once again blue-shifted from 1.83 to 1.88 eV in this case.

ADVANCED
SCIENCE NEWS
www.advancedsciencenews.com

Solar
RRL
www.solar-rrl.com

As with the varied Urbach energy case, an analytical approximation for $\Delta V_{oc,sub-gap}^{rad}$ for the case of a sub-gap EQE_{PV} given by Equation (11) can be obtained assuming that the short-circuit current density is invariant of σ_s and solely determined by the contribution from the above-gap EQE_{PV} (see Section S5 of the Supporting Information). Under such conditions, $\Delta V_{oc,sub-gap}^{rad}$ can be obtained from

$$q\Delta V_{oc,sub-gap}^{rad} \approx \frac{\sigma_s^2}{2kT} + kT\ln\left[\frac{E_{opt}}{3kT}\left(1 - \frac{\sigma_s^2}{E_{opt}kT}\right)^3\right] + kT\ln\left[1 - \left(\frac{qV_{oc}}{E_{opt}}\right)^3\right] \quad (12)$$

where the last term on the right-hand-side is a correction accounting for state filling effects ($w \neq 1$). Equation (12) is indicated by the dashed lines in Figure 3d. As shown, the approximation agrees well with the numerically-calculated results for typical optical gaps.

2.3. Effect of Non-Radiative Open-Circuit Voltage Losses

In real photovoltaic devices, the open-circuit voltage is further reduced by non-radiative recombination, which reduces EQE_{EL} below unity and gives rise to a non-zero non-radiative open-circuit voltage loss ΔV_{oc}^{nr}.[39,42,48] In OPVs, the non-radiative open-circuit voltage loss measured under one Sun has been observed to increase with decreasing energy gap, consistent with the energy-gap law.[39,41,42,48] This is demonstrated in **Figure 4**a, where experimental ΔV_{oc}^{nr} data compiled by Ullbrich et al.[39] are plotted against the energy of the CT state (E_{CT}), which we take as a proxy for E_{opt} (valid for low-offset, NFA OPV blends). Additional ΔV_{oc}^{nr} data for systems with fullerene acceptors and NFAs are plotted as blue squares and green triangles, respectively. We note that at light intensities representative of indoor settings, the non-radiative loss may, in general, be larger (due to additional trap-assisted recombination); as such, the data in

Figure 4a could be considered as an optimistic estimate of ΔV_{oc}^{nr} in organic semiconductor-based IPVs.

To obtain a realistic estimate of non-radiative open-circuit voltage losses in state-of-the-art OPVs, we have designed an empirical, qualitative model for ΔV_{oc}^{nr} based on the experimental data in Figure 4a. In this empirical model, ΔV_{oc}^{nr} is modelled as a quadratic of the form

$$\Delta V_{oc}^{nr} = \begin{cases} AE_{opt}^2 + BE_{opt} + C, & \text{if } E_{opt} \leq 2.601\,eV \\ 0.0945\,V, & \text{otherwise} \end{cases} \quad (13)$$

where the optical gap has units of eV, and the coefficients are $A = 0.123\,V\,(eV)^{-2}$, $B = -0.64\,V\,(eV)^{-1}$, and $C = 0.927\,V$ The transition at 2.601 eV prevents ΔV_{oc}^{nr} from growing again after the parabola reaches its minimum. We stress that this optimistic-yet-realistic model (illustrated by the red curve in Figure 4a) has no underlying theoretical framework and should not be taken as a lower limit for ΔV_{oc}^{nr} in OPVs – it is just a means for encapsulating the general trend shown by the experimental data in Figure 4a. For comparison, another semi-empirical model for ΔV_{oc}^{nr} based on the work of Benduhn et al. is included in Figure 4a.[48] In this model, where a negligibly-small reorganization energy has been assumed, ΔV_{oc}^{nr} relates to E_{CT} via

$$\Delta V_{oc}^{nr} = C - DE_{CT} \approx C - DE_{opt} \quad (14)$$

where $C = 0.574\,V$ and $D = 0.184\,V\,eV^{-1}$. We note that more complex models have been detailed in the literature, including the work of Azzouzi et al. and Chen et al.[41,49]

The effect of the two non-radiative open-circuit voltage loss models on the open-circuit voltage and PCE are illustrated in Figure 4b,c, respectively. To simulate these curves, a step-function EQE_{PV} was used with $EQE_{max} = 0.85$. It is evident from these curves that accounting for realistic non-radiative open-circuit voltage losses reduces the maximum PCE from 45% to around 40%, while blue-shifting the highest-performing optical gap from 1.83 to 1.88 eV. Comparable results are produced by both the semi-empirical energy gap law model given by Equation (14) and the optimistic, empirical model given by
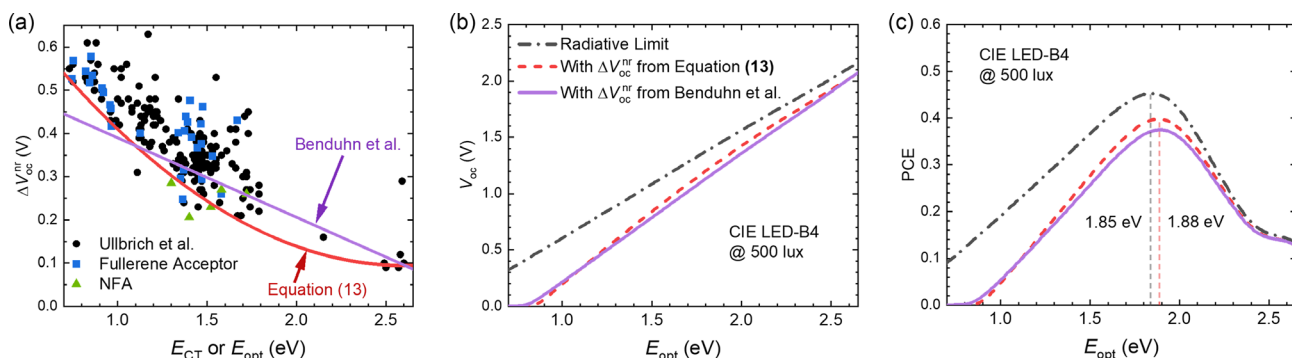

Figure 4. The effect of non-radiative open-circuit voltage losses on the PCE of indoor photovoltaics. a) Non-radiative open-circuit losses as a function of the energy of the CT state, E_{CT}, with experimental data compiled by Ullbrich et al. plotted as black squares.[39] Additional data points for OPV blends with fullerene acceptors and NFAs are plotted as blue squares and green triangles, respectively. The empirical model for ΔV_{oc}^{nr} given by Equation (13) is indicated by the solid red curve, while Benduhn et al.'s empirical model given in Equation (14) is indicated by the purple curve.[48] b) The open-circuit voltage against the optical gap in the radiative limit (black dash-dot curve) and in two non-radiative open-circuit voltage loss models (red dashed curve for Equation (13) and solid purple curve for Equation (14)) calculated using the step function model for EQE_{PV} with $EQE_{max} = 0.85$. c) The resultant power conversion efficiencies under the CIE LED-B4 spectrum at 500 lux.
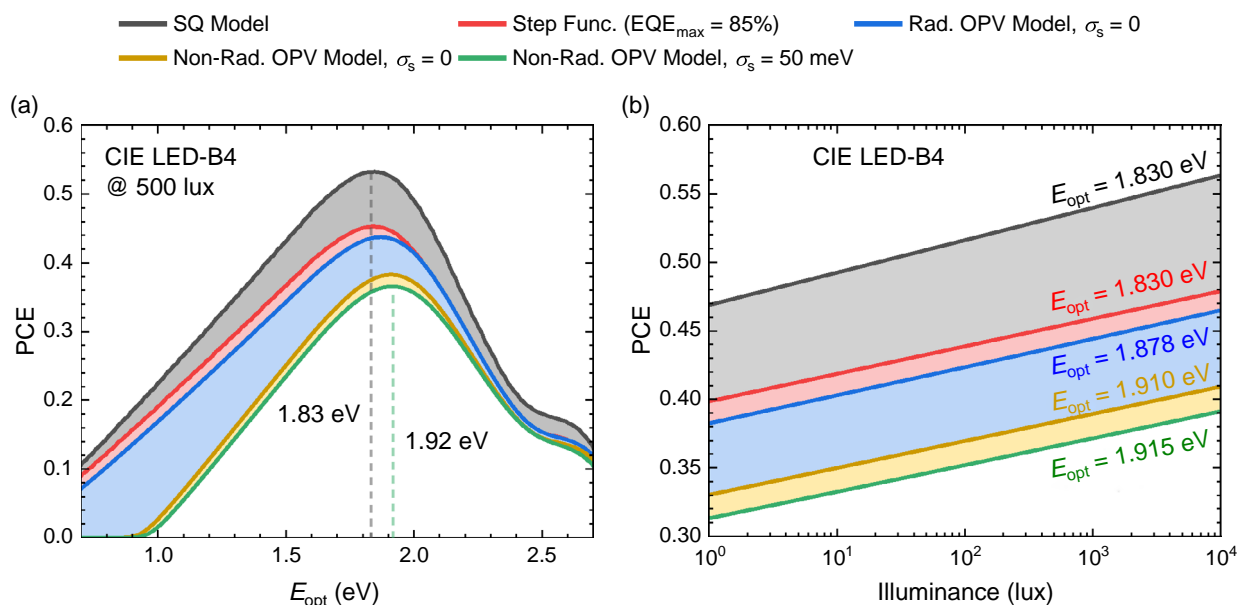
Figure 5. Power conversion efficiencies simulated under the CIE LED-B4 spectrum as a function of the optical gap in (a), and as a function of the illuminance in (b). In both panels, five curves are present. The black curves illustrate the PCE in the radiative SQ Model, while the red curves indicate the PCE when EQE_{PV} is modelled as a step function with $EQE_{max} = 0.85$. The grey shaded regions illustrate the PCE losses induced by non-unity EQE_{max}. The blue, yellow, and green curves, on the other hand, were simulated with modelled using Equation (11) and $EQE_{max} = 0.85$; the blue and yellow curves indicate the $\sigma_s = 0$ case in the radiative and non-radiative limit, respectively, such that the red and blue shaded regions correspond to the losses induced by sub-gap absorption with $E_U = kT$, and non-radiative losses, respectively. In the non-radiative limit, ΔV_{oc}^{nr} is assigned for a given optical gap using Equation (13). Finally, the green curves indicate the non-radiative limit for $\sigma_s = 50$ meV, with the yellow shaded region indicating the additional loss induced by this disorder. In (b), the highest-performing optical gaps used to simulate the curves are inset.

Equation (13). However, as the PCE differs by just a few percent between the models, we herein utilize Equation (13) to model non-radiative losses to make an optimistic prediction for IPV performance.

The predicted PCEs of organic semiconductor-based IPVs, accounting for both radiative losses and non-radiative losses, are shown in **Figure 5** for the CIE LED-B4 spectrum. The OPV predictions (for both $\sigma_s = 0$ and $\sigma_s = 50$ meV) assume sub-gap absorption calculated using Equation (11) and additional ΔV_{oc}^{nr} loss given by Equation (13). Note that $EQE_{max} = 0.85$ was used to predict an optimistic upper limit for OPVs. For comparison, the ideal radiative PCE limits based on the step-function model (Equation (7)) with $EQE_{max} = 1$ (i.e., the SQ model) and the more realistic $EQE_{max} = 0.85$ have been included to indicate the performance loss across all optical gaps. These five curves are plotted against the optical gap at an illuminance of 500 lux in Figure 5a, whereas, in Figure 5b, they are plotted against the illuminance of the incident light for the best-performing optical gap (which has been inset into the graph for each curve).

By accounting for sub-gap absorption, energetic disorder, and realistic non-radiative open-circuit voltage losses, we find that the maximum PCE of OPVs under CIE LED-B4 at 500 lux is reduced from its SQ model value of 53% to around 37%. Furthermore, the highest-performing E_{opt} is blue-shifted by around 90 meV. Corresponding discussions for the 2700 K LED and 4000 K LED sources are provided in Section S6 of the Supporting Information. Additionally, similar figures for three standard fluorescent sources (CIE FL-2, CIE FL-7, and CIE FL-11) are

illustrated in Figure S8 of the Supporting Information. We note again that the simulated results are mostly independent of the source of artificial light.

Based on Figure 5, an OPV blend with the highest-performing optical gap of $E_{opt} = 1.92$ eV and minimal energetic disorder will likely have a PCE lower than 40% at typical indoor light intensities (up to 5000 lux). Accounting for energetic disorder (typically on the order of $\sigma_s = 50$ meV) further reduces the PCE. To estimate the figures-of-merit of particular OPV materials in indoor settings more accurately, we have devised a methodology and created an associated computational tool with an accessible graphical user interface (available as Supporting Information)[50] that takes an experimentally-determined EQE_{PV} spectrum and measured open-circuit voltage under one Sun ($V_{oc}^{\odot}$) as inputs. We stress that similar approaches for predicting IPV performance using EQE_{PV} and current-voltage measurements have been established in the past (see, e.g., the work of Lübke et al.[18]). In our case, however, we focus on predicting upper performance limits using measured EQE_{PV} spectra, which account for sub-gap absorption in real OPV systems. Using a device's EQE_{PV} spectrum and $V_{oc}^{\odot}$, the non-radiative open-circuit voltage loss is estimated through

$$\Delta V_{oc}^{nr} \approx \frac{k_B T}{q} \ln\left(1 + \frac{J_{sc}^{\odot}}{J_0^{rad}}\right) - V_{oc}^{\odot} \tag{15}$$

where $J_{sc}^{\odot}$ is the short-circuit current density under one Sun (determined using EQE_{PV}). Assuming Equation (15) provides
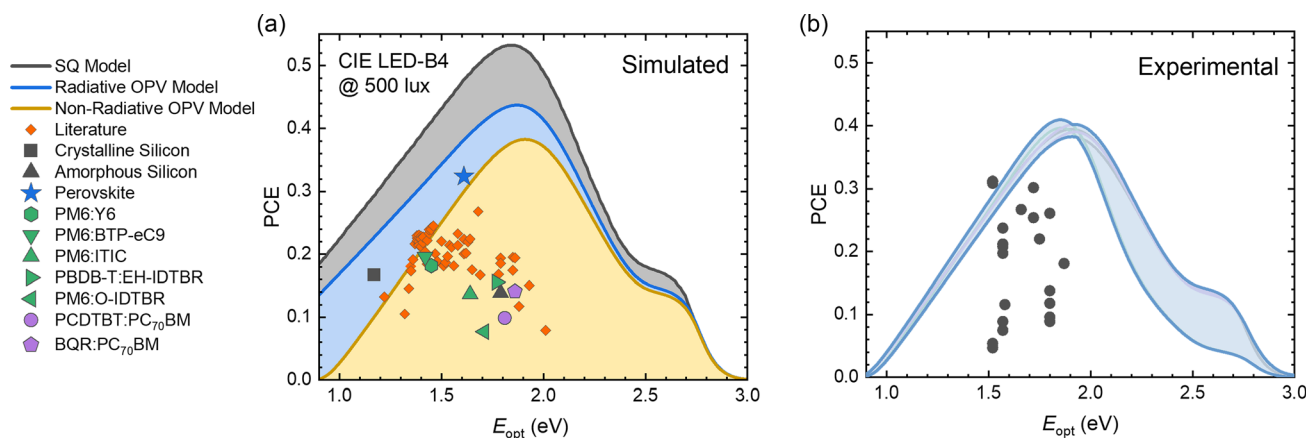
Figure 6. Power conversion efficiencies under indoor lighting conditions. a) A comparison of the predicted indoor performance of OPV systems (Almora et al. systems in orange,[52,53] additional fullerene acceptor and NFA systems in green and purple, respectively), crystalline and amorphous silicon (black data points) and a perovskite (blue star), with the PCE in the SQ model (black curve), and in the radiative and non-radiative OPV predictions in the limit of $\sigma_s = 0$ (shown by the blue and gold curves, respectively). The blue shaded region indicates a regime of optimal performance for materials with low energetic disorder and low ΔV_{oc}^{nr}, whereas the gold shaded region indicates a realistic regime for disordered OPV systems with medium-to-high ΔV_{oc}^{nr}. b) Experimental PCEs under LED sources from the literature (see Table S6 of the Supporting Information), compared with the non-radiative OPV model as a function of the optical gap for the CIE LED-B4, 2700 K LED, and 4000 K LED sources, at both 500 lux and 2000 lux in the hypothetical $\sigma_s = 0$ case.

a realistic lower limit estimate of the device's ΔV_{oc}^{nr}, optimistic values for the photovoltaic figures-of-merit can then be estimated under any spectrum at any intensity. A block diagram detailing this methodology, including the identification of the true radiative open-circuit voltage in the thermodynamic limit, is shown in Figure S9 of the Supporting Information.

2.4. Comparative Analysis

In **Figure 6**a, the PCE is plotted in the SQ model and in both the radiative limit (blue curve) and non-radiative limit (gold curve) of the more realistic OPV model (in the case that $\sigma_s = 0$), where EQE_{PV} is modelled using Equation (11). For the non-radiative case the ΔV_{oc}^{nr} is assumed to be given by Equation (13). Also shown are the predicted PCEs of a wide range of OPVs,[8,31,51–56] crystalline and amorphous silicon,[51,57] and perovskite[55] under CIE LED-B4 (see Table S5 in the Supporting Information). These predictions were made using each system's EQE_{PV} spectrum and $V_{oc}^{\odot}$ from the literature, with the optical gaps taken from the tables of Almora et al.[52,53] Where sensitive EQE_{PV} measurements were available, however, the optical gaps were determined using Equation (11) via the technique summarized in Section S8 of the Supporting Information.[33]

From the estimated PCEs of Figure 6a, it is evident that the state-of-the-art organic solar cell blends PM6:Y6 and PM6:BTP-eC9 (with $E_{opt}\sim1.4$eV) will likely not exceed PCEs of 20% in indoor settings unless the non-radiative losses can be drastically reduced. As previously discussed in Figure 5, this becomes more evident when accounting for energetic disorder (around 43 meV for both blends) as it further reduces the radiative limit. On the other hand, other OPV systems such as PBDB-T:EH-IDTBR and PM6:O-IDTBR, have a fair amount of room for improvement. This is particularly clear when comparing with experimentally-determined PCE values from the literature, as evidenced in Figure 6b (see Table S5 of the Supporting Information; all plotted

PCEs were measured at 2000 lux or less).[19,29,58–63] Alongside this data, the PCE predicted by the realistic, non-radiative OPV model (with $\sigma_s = 0$) has been plotted for the CIE LED-B4, 2700 K LED, and 4000 K LED spectra at both 500 and 2000 lux. An envelope has then been plotted to encapsulate the minimum and maximum PCE held by any of the spectra at each optical gap, providing a realistic estimate for the PCE of IPVs under any LED spectrum.

Based on Figure 6, we can see that many of the OPV blends have room for improvement. We also note, however, that at least one data point from the literature defies the realistic OPV limit with reasonable non-radiative loss, despite the fact that the simulations were conducted at a higher illuminance. Possible reasons for this deviation might be related to 1) inaccuracies in the estimated optical gap; 2) a very small non-radiative voltage loss in this OPV system, especially as Equation (13) predicts a larger ΔV_{oc}^{nr} than some of the literature data in Figure 4a, and/or iii) inaccuracies in the experimental set-up as previously discussed by Lübke et al.[18] Case studies like this demonstrate not only the challenging task of measuring indoor PCEs, but also the dire need for a tried and tested standard for IPVs, including an accepted experimental methodology for characterizing the devices.

3. Conclusion

IPVs are rapidly proving to be a very practical application for organic semiconductors; they continue to be a promising contender for powering for the IoT using energy-harvesting techniques. There are, however, some inconsistencies in the literature regarding the PCEs of IPVs likely due to a lack of an accepted testing standard for IPVs. By presenting a realistic limit for the PCE of OPVs, which accounts for both radiative open-circuit voltage losses induced by sub-gap absorption (including Urbach tails and energetic disorder) and non-radiative

open-circuit voltage losses, we aim to elucidate what PCEs could reasonably be expected. In particular, we have shown that a combination of realistic above-gap EQE_{PV} and ΔV_{oc}^{nr}, in combination with a typical energetic disorder ($\sigma_s = 50\,meV$), can reduce the maximum PCE of OPVs from a SQ model value of 53% to $\approx 37\%$ under indoor lighting conditions. We have also shown that the best-performing optical gap becomes blue-shifted from $E_{opt} = 1.83$ to $1.92\,eV$ for $\sigma_s = 50\,meV$, suggesting that the high-performance OPV blends PM6:Y6 and PM6:BTP-eC9 may not exceed PCEs of 20% in indoor settings. To aid future work on indoor applications of OPVs, we have presented a methodology for estimating the performance of IPVs at typical illuminances, using measurements of the photovoltaic external quantum efficiency spectrum and the open-circuit voltage under one Sun. Furthermore, to automate the estimation of IPV performance under arbitrary illumination conditions using these quantities, we have provided a computational tool (with a graphical user interface) as Supporting Information.[50]

4. The Computational Tool

To aid the estimation of the PCEs of particular photovoltaic materials, a computational tool was prepared in the open-source Python interactive development environment, Jupyter, see ref. [50]. While this is not the first computational tool for simulating photovoltaic figures-of-merit under indoor illumination conditions, it does have a few unique characteristics. Chief among these, this tool includes a detailed graphical user interface that can be used to control the simulations. To estimate IPV device performance, the tool allows the use of both simulated and experimentally-determined EQE_{PV} spectra; it can simulate step-functions, sub-gap Urbach tails, and OPV absorption using Equation (11). Using these simulated EQE_{PV} spectra, the tool determines the photovoltaic figures-of-merit under a selected spectrum (e.g., CIE LED-B4) at any desired illuminance. A variety of non-radiative open-circuit voltage loss models are also available, including Equation (13). The photon flux spectra used by the tool can be customized (and superimposed), and as many EQE_{PV} spectra as desired can be loaded in. These spectra may be analyzed individually, or countless systems may be analyzed at once in bulk – enabling a prediction of which device would perform best out of a selection of hundreds under a given spectrum in a matter of seconds. The tool is applicable to any class of semiconductor materials, including organics, inorganics, and perovskites. Alongside the well-detailed tool, a manual has also been prepared that describes how to install Jupyter and how to navigate the user interface.[50]

Supporting Information

Supporting Information is available from the Wiley Online Library or from the author.

Acknowledgements

Conflict of Interest

The authors declare no conflict of interest.

Data Availability Statement

The data that support the findings of this study are available from the corresponding author upon reasonable request.

[1] L. Atzori, A. Iera, G. Morabito, *Comput. Networks* **2010**, *54*, 2787.
[2] O. Vermesan, P. Friess, P. Guillemin, R. Giaffreda, H. Grindvoll, M. Eisenhauer, M. Serrano, K. Moessner, M. Spirito, L.-C. Blystad, in *Building the Hyperconnected Society-Internet of Things Research and Innovation Value Chains, Ecosystems and Markets*, River Publishers, New York, NY **2015**, pp. 15–118.
[3] Intel, Intelligent Decisions with Intel Internet of Things (IoT), https://www.intel.co.uk/content/www/uk/en/internet-of-things/overview.html (accessed: January 2023).
[4] R. Arshad, S. Zahoor, M. A. Shah, A. Wahid, H. Yu, *IEEE Access* **2017**, *5*, 15667.
[5] S. H. Alsamhi, O. Ma, M. Ansari, Q. Meng, *Telecommun. Syst.* **2019**, *72*, 609.
[6] V. Rozite, et al., *More Data, Less Energy*, International Energy Agency, Paris, France **2014**.
[7] V. Pecunia, L. G. Occhipinti, R. L. Z. Hoye, *Adv. Mater.* **2021**, *11*, 2100698.
[8] G. Burwell, O. J. Sandberg, W. Li, P. Meredith, M. Carnie, A. Armin, *Sol. RRL* **2022**, *6*, 2200315.
[9] M. Freunek, M. Freunek, L. M. Reindl, *IEEE J. Photovoltaics* **2012**, *3*, 59.
[10] A. Ndiaye, A. Charki, A. Kobi, C. M. F. Kébé, P. A. Ndiaye, V. Sambou, *Sol. Energy* **2013**, *96*, 140.
[11] J. A. Nelson, *The Physics of Solar Cells*, Imperial College Press, London, UK **2003**.
[12] J. K. W. Ho, H. Yin, S. K. So, *J. Mater. Chem. A* **2020**, *8*, 1717.
[13] W. Shockley, H. J. Queisser, *J. Appl. Phys.* **1961**, *32*, 510.
[14] C. Sprau, F. Buss, M. Wagner, D. Landerer, M. Koppitz, A. Schulz, D. Bahro, W. Schabel, P. Scharfer, A. Colsmann, *Energy Environ. Sci.* **2015**, *8*, 2744.
[15] R. Abbel, Y. Galagan, P. Groen, *Adv. Eng. Mater.* **2018**, *20*, 1701190.
[16] H. K. H. Lee, Z. Li, J. R. Durrant, W. C. Tsoi, *Appl. Phys. Lett.* **2016**, *108*, 253301.

[17] D. Lübke, P. Hartnagel, M. Hülsbeck, T. Kirchartz, *ACS Materi. Au* **2023**, *3*, 215.

[18] D. Lübke, P. Hartnagel, J. Angona, T. Kirchartz, *Adv. Mater.* **2021**, *11*, 2101474.

[19] Y. Cui, Y. Wang, J. Bergqvist, H. Yao, Y. Xu, B. Gao, C. Yang, S. Zhang, O. Inganäs, F. Gao, J. Hou, *Nat. Energy* **2019**, *4*, 768.

[20] A. Armin, W. Li, O. J. Sandberg, Z. Xiao, L. Ding, J. Nelson, D. Neher, K. Vandewal, S. Shoaee, T. Wang, H. Ade, T. Heumüller, C. Brabec, P. Meredith, *Adv. Mater.* **2021**, *11*, 2003570.

[21] J. Hou, O. Inganäs, R. H. Friend, F. Gao, *Nat. Mater.* **2018**, *17*, 119.

[22] S. Liu, J. Yuan, W. Deng, M. Luo, Y. Xie, Q. Liang, Y. Zou, Z. He, H. Wu, Y. Cao, *Nat. Photonics* **2020**, *14*, 300.

[23] A. Colsmann, H. Röhm, C. Sprau, *Sol. RRL* **2020**, *4*, 2000015.

[24] Z. Genene, W. Mammo, E. Wang, M. R. Andersson, *Adv. Mater.* **2019**, *31*, 1807275.

[25] O. Inganäs, *Adv. Mater.* **2018**, *30*, 1800388.

[26] Y. Cui, L. Hong, J. Hou, *ACS Appl. Mater. Interfaces* **2020**, *12*, 38815.

[27] B. Minnaert, P. Veelaert, *Energies* **2014**, *7*, 1500.

[28] X. Hou, Y. Wang, H. K. H. Lee, R. Datt, N. Uslar Miano, D. Yan, M. Li, F. Zhu, B. Hou, W. C. Tsoi, Z. Li, *J. Mater. Chem. A* **2020**, *8*, 21503.

[29] L.-K. Ma, Y. Chen, P. C. Y. Chow, G. Zhang, J. Huang, C. Ma, J. Zhang, H. Yin, A. M. Hong Cheung, K. S. Wong, S. K. So, H. Yan, *Joule* **2020**, *4*, 1486.

[30] Y. Zhang, C. Duan, L. Ding, *Sci. Bull* **2020**, *65*, 10.1016.

[31] C. Kaiser, O. J. Sandberg, N. Zarrabi, W. Li, P. Meredith, A. Armin, *Nat. Commun.* **2021**, *12*, 3988.

[32] S. Hood, N. Zarrabi, P. Meredith, I. Kassal, A. Armin, *J. Phys. Chem. Lett.* **2019**, *10*, 3863.

[33] A. M. Kay, O. J. Sandberg, N. Zarrabi, W. Li, S. Zeiske, C. Kaiser, P. Meredith, A. Armin, *Adv. Funct. Mater.* **2022**, *32*, 2113181.

[34] J. Wu, J. Luke, H. K. H. Lee, P. Shakya Tuladhar, H. Cha, S.-Y. Jang, W. C. Tsoi, M. Heeney, H. Kang, K. Lee, T. Kirchartz, J.-S. Kim, J. R. Durrant, *Nat. Commun.* **2019**, *10*, 5159.

[35] F. Urbach, *Phys. Rev.* **1953**, *92*, 1324.

[36] J. Wong, S. T. Omelchenko, H. A. Atwater, *ACS Energy Lett.* **2020**, *6*, 52.

[37] J. Yan, E. Rezasoltani, M. Azzouzi, F. Eisner, J. Nelson, *Nat. Commun.* **2021**, *12*, 3642.

[38] S. Beuel, P. Hartnagel, T. Kirchartz, *Adv. Theor Simul.* **2021**, *4*, 2000319.

[39] S. Ullrich, J. Benduhn, X. Jia, V. C. Nikolis, K. Tvingstedt, F. Piersimoni, S. Roland, Y. Liu, J. Wu, A. Fischer, D. Neher, S. Reineke, D. Spoltore, K. Vandewal, *Nat. Mater.* **2019**, *18*, 459.

[40] T. Kirchartz, K. Taretto, U. Rau, *J. Phys. Chem. C* **2009**, *113*, 17958.

[41] M. Azzouzi, J. Yan, T. Kirchartz, K. Liu, J. Wang, H. Wu, J. Nelson, *Phys. Rev. X* **2018**, *8*, 031055.

[42] U. Rau, *Phys. Rev. B* **2007**, *76*, 085303.

[43] CIE, Relative Spectral Power Distributions of Illuminants Representing Typical Fluorescent Lamps, 1nm Wavelength Steps, **2018**, https://cie.co.at/datatable/relative-spectral-power-distributions-illuminants-representing-typical-fluorescent-lamps-0 (accessed: May 2023).

[44] CIE, Relative Spectral Power Distributions of Illuminants Representing Typical LED Lamps, 1nm Spacing, **2018**, https://cie.co.at/datatable/relative-spectral-power-distributions-illuminants-representing-typical-led-lamps-1nm (accessed: May 2023).

[45] P. Würfel, U. Würfel, *Physics of Solar Cells: From Basic Principles to Advanced Concepts*, John Wiley & Sons, Weinheim, Germany **2016**.

[46] W. Gong, M. A. Faist, N. J. Ekins-Daukes, Z. Xu, D. D. C. Bradley, J. Nelson, T. Kirchartz, *Phys. Rev. B* **2012**, *86*, 024201.

[47] U. Rau, B. Blank, T. C. M. Müller, T. Kirchartz, *Phys. Rev. Appl.* **2017**, *7*, 044016.

[48] J. Benduhn, K. Tvingstedt, F. Piersimoni, S. Ullrich, Y. Fan, M. Tropiano, K. A. McGarry, O. Zeika, M. K. Riede, C. J. Douglas, S. Barlow, S. R. Marder, D. Neher, D. Spoltore, K. Vandewal, *Nat. Energy* **2017**, *2*, 17053.

[49] X.-K. Chen, D. Qian, Y. Wang, T. Kirchartz, W. Tress, H. Yao, J. Yuan, M. Hülsbeck, M. Zhang, Y. Zou, Y. Sun, Y. Li, J. Hou, O. Inganäs, V. Coropceanu, J.-L. Bredas, F. Gao, *Nat. Energy* **2021**, *6*, 799.

[50] The Computational Tool is Freely Available, https://github.com/Austin-M-Kay/Photovoltaic_Performance_Simulator.

[51] N. Zarrabi, O. J. Sandberg, S. Zeiske, W. Li, D. B. Riley, P. Meredith, A. Armin, *Nat. Commun.* **2020**, *11*, 5567.

[52] O. Almora, D. Baran, G. C. Bazan, C. Berger, C. I. Cabrera, K. R. Catchpole, S. Erten-Ela, F. Guo, J. Hauch, A. W. Y. Ho-Baillie, T. J. Jacobsson, R. A. J. Janssen, T. Kirchartz, N. Kopidakis, Y. Li, M. A. Loi, R. R. Lunt, X. Mathew, M. D. McGehee, J. Min, D. B. Mitzi, M. K. Nazeeruddin, J. Nelson, A. F. Nogueira, U. W. Paetzold, N.-G. Park, B. P. Rand, U. Rau, H. J. Snaith, E. Unger, L. Vaillant-Roca, H.-L. Yip, C. J. Brabec, *Adv. Mater.* **2021**, *11*, 2102526.

[53] O. Almora, D. Baran, G. C. Bazan, C. I. Cabrera, S. Erten-Ela, K. Forberich, F. Guo, J. Hauch, A. W. Y. Ho-Baillie, T. J. Jacobsson, R. A. J. Janssen, T. Kirchartz, N. Kopidakis, M. A. Loi, R. R. Lunt, X. Mathew, M. D. McGehee, J. Min, D. B. Mitzi, M. K. Nazeeruddin, J. Nelson, A. F. Nogueira, U. W. Paetzold, B. P. Rand, U. Rau, H. J. Snaith, E. Unger, L. Vaillant-Roca, C. Yang, H.-L. Yip, C. J. Brabec, *Adv. Mater.* **2023**, *13*, 2203313.

[54] S. Zeiske, C. Kaiser, P. Meredith, A. Armin, *ACS Photonics* **2020**, *7*, 256.

[55] S. Zeiske, O. J. Sandberg, N. Zarrabi, C. M. Wolff, M. Raoufi, F. Peña-Camargo, E. Gutierrez-Partida, P. Meredith, M. Stolterfoht, A. Armin, *J. Phys. Chem. Lett.* **2022**, *13*, 7280.

[56] W. Li, S. Zeiske, O. J. Sandberg, D. B. Riley, P. Meredith, A. Armin, *Energy Environ. Sci.* **2021**, *14*, 6484.

[57] S. Jeong, M. D. McGehee, Y. Cui, *Nat. Commun.* **2013**, *4*, 2950.

[58] D. Su, M.-A. Pan, Z. Liu, T.-K. Lau, X. Li, F. Shen, S. Huo, X. Lu, A. Xu, H. Yan, C. Zhan, *Chem. Mater.* **2019**, *31*, 8908.

[59] T. Zhang, C. An, Y. Xu, P. Bi, Z. Chen, J. Wang, N. Yang, Y. Yang, B. Xu, H. Yao, X. Hao, S. Zhang, J. Hou, *Adv. Mater.* **2022**, *34*, 2207009.

[60] S. V. Dayneko, M. Pahlevani, G. C. Welch, *ACS Appl. Mater. Interfaces* **2019**, *11*, 46017.

[61] S. Mori, T. Gotanda, Y. Nakano, M. Saito, K. Todori, M. Hosoya, *Jpn. J. Appl. Phys.* **2015**, *54*, 071602.

[62] X. Zhou, H. Wu, U. Bothra, X. Chen, G. Lu, H. Zhao, C. Zhao, Q. Luo, G. Lu, K. Zhou, D. Kabra, Z. Ma, W. Ma, *Mater. Horiz.* **2023**, *10*, 566.

[63] C. Lee, J.-H. Lee, H. H. Lee, M. Nam, D.-H. Ko, *Adv. Mater.* **2022**, *12*, 2200275.